Growth couples temporal and spatial fluctuations of tissue properties during morphogenesis

Antoine Fruleux, Lilan Hong, Adrienne H K Roeder, Chun-Biu Li, Arezki Boudaoud

Growth couples temporal and spatial fluctuations of tissue properties during morphogenesis

Antoine Fruleux*
RDP, Université de Lyon, ENS de Lyon, UCB Lyon 1, INRAE, CNRS, 69364 Lyon Cedex 07, France
LadHyX, CNRS, Ecole polytechnique, Institut Polytechnique de Paris, 91128 Palaiseau Cedex, France and
LPTMS, CNRS, Université Paris-Saclay, 91405, Orsay, France.

Lilan Hong
Institute of Nuclear Agricultural Sciences, Key Laboratory of Nuclear Agricultural Sciences of Ministry of Agriculture and Zhejiang Province, College of Agriculture and Biotechnology, Zhejiang University, Hangzhou, Zhejiang 310058, China.

Adrienne H. K. Roeder
Weill Institute for Cell and Molecular Biology and Section of Plant Biology, School of Integrative Plant Science; Cornell University, Ithaca, New York 14853, USA

Chun-Biu Li
Department of Mathematics, Stockholm University, 106 91 Stockholm, Sweden

Arezki Boudaoud†
RDP, Université de Lyon, ENS de Lyon, UCB Lyon 1, INRAE, CNRS, 69364 Lyon Cedex 07, France and
LadHyX, CNRS, Ecole polytechnique, Institut Polytechnique de Paris, 91128 Palaiseau Cedex, France
(Dated: October 23, 2023)

Living tissues display fluctuations – random spatial and temporal variations of tissue properties around their reference values – at multiple scales. It is believed that such fluctuations may enable tissues to sense their state or their size. Recent theoretical studies developed specific models of fluctuations in growing tissues and predicted that fluctuations of growth show long-range correlations. Here we elaborated upon these predictions and we tested them using experimental data. We first introduced a minimal model for the fluctuations of any quantity that has some level of temporal persistence or memory, such as concentration of a molecule, local growth rate, or mechanical properties. We found that long-range correlations are generic, applying to to any such quantity, and that growth couples temporal and spatial fluctuations. We then analysed growth data from sepals of the model plant Arabidopsis and we quantified spatial and temporal fluctuations of cell growth using the previously developed Cellular Fourier Transform. Growth appears to have long-range correlations. We compared different genotypes and growth conditions: mutants with altered response to mechanical stress have lower temporal correlations and longer-range spatial correlations than wild-type plants. Finally, we used a theoretical prediction to collapse experimental data from all conditions and developmental stages, validating the notion that temporal and spatial fluctuations are coupled by growth. Altogether, our work reveals kinematic constraints on spatiotemporal fluctuations that have an impact on the robustness of morphogenesis.

Significance Statement

How do organs and organisms grow and achieve robust shapes in the face of subcellular and cellular variability is still a mystery. Here we investigated the variability of growth at multiple scales and we analysed experimental growth data from growing plant tissues. Our results support the prediction that tissue expansion couples temporal memory of growth with spatial variability of growth. Our work reveals a constraint on spatiotemporal variability of growth that may impact the robustness of morphogenesis.

INTRODUCTION

The impact of noisy perturbations on organism development is the subject of active research [1]. Fluctuations – the random spatial and temporal variations of tissue properties around their reference values – are observed at multiple scales, from cytoskeleton [2] to cell [3] and

* antoine.fruleux@universite-paris-saclay.fr
† arezki.boudaoud@polytechnique.edu

tissue [4]. It has been proposed that fluctuations are required for symmetry breaking and pattern formation during development [5, 6] or for cells and tissues to sense their neighbourhood [7]. Fluctuations in growth induce mechanical stress [7–10] because, for instance, cells with higher growth rate exert forces on neighbouring cells, which may sense and respond to such mechanical stress. Robust development of the fruit fly wing partially relies on cell competition, i.e. on mismatch of growth rates between cells, and on the ensuing modulation of proliferation and apoptosis [11, 12]. In this context, it is important to understand whether fluctuations of a cell affect its local neighbourhood or the whole tissue. Here, we analysed the spatial structure of fluctuations in experimental data from growing tissues.

Recent models of tissue mechanics and growth accounted for temporal and spatial fluctuations of growth and investigated their role in robustness of morphogenesis [13–15]. Temporal fluctuations are characterised by their degree of persistence, quantified with the persistence time (or correlation time), the characteristic time over which memory of previous fluctuations is lost. It could be the time needed for remodelling of the cytoskeleton or of the extra-cellular matrix (in animals) / the cell wall (in plants). Spatial fluctuations are characterised by their degree of spatial consistency, quantified by the correlation length, the characteristic length over which cells (or subcellular domains) behave similarly, or by cell-to-cell variability over a small neighbourhood. For instance, the shape of a plant lateral organ was found to be less robust in a mutant with lower cell-to-cell variability [13]. However, the spatial fluctuations may have a more complex structure. Indeed, theoretical models of the expanding universe [16, 17] and of growing tissues [14, 15] predict long-range spatial correlations, i.e. a significant level of correlations between fluctuations of two distant parts of the system; accordingly, growing systems are expected to exhibit fluctuations at multiple scales. Here we focus on the underlying mechanism, which we call fluctuation stretching – the increase in the lengthscale of fluctuations of a tissue property or of the concentration of a molecule, due to tissue expansion.

To assess the experimental relevance of this mechanism, we analyzed growth fluctuations in the model plant *Arabidopsis thaliana*. We considered the sepal, the green leaf-like organ that protects a flower prior to their opening. We characterised sepals from wild-type individuals in different culture conditions as well as mutant plants. We considered *spiral2* and *katanin* mutant plants since they were found less robust to the variability in the number of trichomes (hair cells) than wild types plants [18], suggesting a greater impact of cellular scales on organ ones. The lack of SPIRAL2 and KATANIN function lead respectively to stronger [18–20] and weaker [18, 19, 21] cortical microtubule co-alignment and reorientation in response to mechanical stress [22, 23]. Microtubules guide the deposition of cellulose fibers in the cell wall (the plant extra-cellular matrix) [24]. Cellulose fibers being the main load-bearing component of the cell wall, the response of microtubules to stress is generally considered as a mechanical feedback on growth and *spiral2* and *katanin* as mutants with altered feedback.

In this Article, we first present a simple model for fluctuation stretching. We estimate spatial and temporal correlations of tissue growth fluctuations in Arabidopsis sepals using previous live imaging data [18, 19] and the Cellular Fourier Transform (CFT) [25]. We investigate how correlations vary within and between datasets and we test the existence of the fluctuation stretching mechanism.

RESULTS

Models predict the stretching of fluctuations in growing tissues

Fluctuation stretching, the enlargement of the lengthscale of fluctuations by medium expansion, is predicted by different models of expanding media, the early universe [16] and living tissues [14, 15]. Fluctuation stretching can be understood with the help of FIG.1 and is formally derived in section Datasets and Methods. Panel **A** depicts the relaxation towards equilibrium of a variable with a spatial pattern on a growing tissue; this variable could reflect gene expression, signalling, metabolism, cell size or cell growth, for instance. If the pattern is temporally persistent, the lengthscale of spatial variations will be enlarged under the effect of growth, while the amplitude of the pattern will be maintained or reduced over time depending on whether the persistence is complete or partial, respectively. In the absence of temporal persistence, the pattern disappears at the next time point. In the presence of a noise source, the pattern caused by the source at a given time point superimposes to the preexisting patterns that have been stretched by growth from previous time points. Altogether, fluctuations of the variable of interest correspond to a mixture of patterns with different lengthscales with weight parameterized by the persistence time τ and by average growth rate $\overline{G}$; the more fluctuations persist over the time for the tissue to double in size (characteristic time of growth), the more weight is taken by fluctuations that vary over large lengthscales. This relation can be made quantitative by using correlation functions.

The space correlation function, $C(l)$, is the pairwise correlation between the values $\Phi(x)$ and $\Phi(x+l)$ of a variable Φ at positions distant of length l, as illustrated in FIG. 1 **B**. $C(l)$ generally decrease with the distance l: for $l = 0$, $\Phi(x) = \Phi(x+l)$ and so the correlation is complete, $C(0) = 1$, while at large distance l, $\Phi(x + l)$ is expected to be independent of $\Phi(x)$ and the correlation vanishes as illustrated in the plot on the right of panel **B**. FIG.1 **C-E** show the predicted space correlation functions for fully, partially, and no time persistent fluctuations. Because of fluctuation stretching, space correlations func-

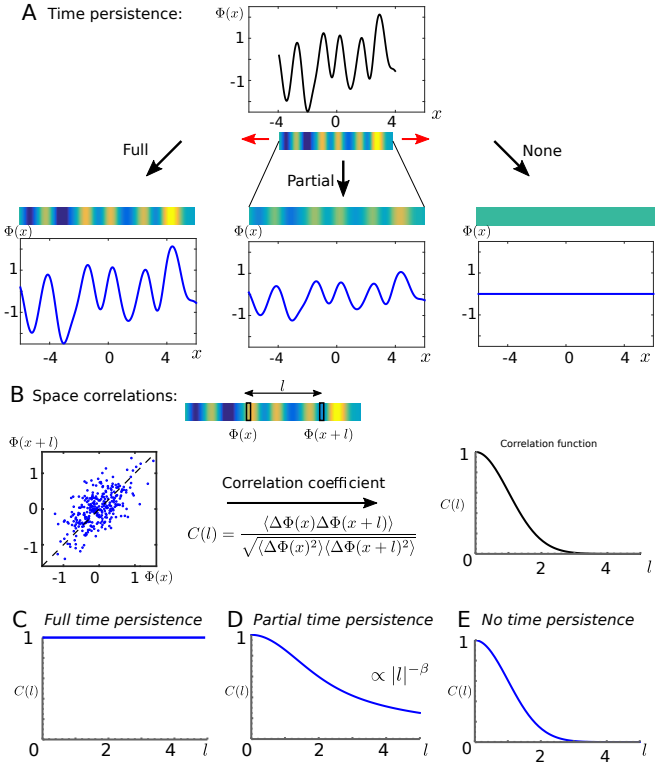

FIG. 1. An explanation of 'fluctuation stretching', defined as the enlargement of the lengthscale of fluctuations by tissue expansion. The resulting spatial correlations depend on the level of temporal persistence of fluctuations. Three levels of temporal persistence are considered here: full, intermediate, and none. **A** Initial spatial pattern and its temporal evolution for the three levels of temporal persistence. The variable $\Phi(x)$ is plotted as a function of position x and shown in colorscale (blue and yellow for low and high values, respectively) along a strip standing for the growing tissue. The red arrows indicate the direction of expansion. **B** Quantification of spatial correlations. Top: This involves comparing the values of the variable at positions x and $x+l$, as illustrated in the colored strip. Left: Typical scatter plot showing $\Phi(x+l)$ as a function of $\Phi(x)$ for multiple values of x. Middle: $C(l)$ is defined as the correlation coefficient between $\Phi(x+l)$ and $\Phi(x)$; $\langle\cdot\rangle$ stands for the average over the dataset of the expression is between the brackets and $\Delta\Phi(x) = \Phi(x) - \langle\Phi(x)\rangle$. Left: the correlation $C(l)$ as a function of the distance l. **C-E** Spatial correlation function $C(l)$ for full, partial, and no time persistent fluctuations. Models predict that the space correlation function is a power-law of l, $C(l) \propto l^{-\beta}$.

tions for time persistent fluctuations are predicted to be long-ranged *i.e.* to have their tails which follow a power law $\propto l^{-\beta}$ provided that there is a permanent noise source and that G and τ remain stationary in time. This scaling law reflects that fluctuations are a superimposition of patterns with different spatial lengthscales: the larger $\tau\overline{G}$, the higher correlations between distant regions. Full temporal persistence is simply the limit where the persistence time is infinite, so that the correlation function is constant, whereas in the absence of temporal persistence, spatial correlations vanish beyond the correlation length of the noise source. In section Datasets and Methods (together with the Supplementary note), we used a simple model to show that fluctuation stretching relates the exponent of the correlation function to the dimension of space ($D = 1$ in the illustrative figure, $D = 2$ for thin organs such as sepals), the persistence time, and average growth rate:

$$\beta = \frac{2D}{\tau\overline{G}}. \quad (1)$$

Here, we tested this prediction using previous experimental data about growing plant organs.

Live imaging and spectral analysis provide estimates for spatiotemporal correlations of cell growth

Next we aimed at a quantitative description of spatial and temporal correlations of growth fluctuations in expanding tissues. We used experimental data where sepals were imaged live to track morphogenesis over time, with similar culture and imaging conditions [18, 19]. We examined whether fluctuations stretching applies to cell areal growth rate. Each sepal was imaged at multiple times, labeled $t = 0, 1, 2, ...$ and separated by 24 hours intervals as illustrated by FIG.2**A**, which shows an example of cells segmented in a sepal, at three successive time steps t, $t+1$ and $t+2$. Growth was defined from the cell surface area at successive time steps. FIG.2**B** shows cell areal relative growth rate $G_{i,t}$ and $G_{i,t+1}$ from t to $t+1$ and from $t+1$ to $t+2$ respectively, deduced from the segmentations showed in panel **A** and mapped on the reference tissues at t and $t+1$, respectively. When a cell has divided between t to $t+1$, we used the total surface area of the daughter cells at $t+1$ to define $G_{i,t}$. (The explicit form of $G_{i,t}$ is given in section Datasets ans Methods.)

To dissect spatial variations of growth in the tissue, we used the Cellular Fourier Transform (CFT) [25]. The CFT consists of decomposing the signal into a linear combination of ad hoc harmonics that account for the subdivision of the tissue into cells of variable size and shape. These harmonics are the equivalent of sinusoidal waves in an infinite continuous medium. The k-th harmonic, e_k, has wavenumber q_k, and varies on a lengthscale that increases with the rank k, which enable the multi-scale decomposition of signals defined over the tissue. The CFT $\hat{G}_{k,t}$ gives the weights with which cell relative areal growth is decomposed into the harmonics e_k. Fourier spectra are obtained by plotting the amplitudes $|\hat{G}_{k,t}|$ as a function the corresponding wave number q_k. These spectra are well-suited to describe fluctuations in a tissue at multiple scales.

We estimated spatial correlations from Fourier spectra such as those shown in FIG.2.**D**$_1$-**D**$_2$, which show that growth fluctuates at multiple scales. The prediction of long-range correlations, $C(l) \sim l^{-\beta}$, corresponds

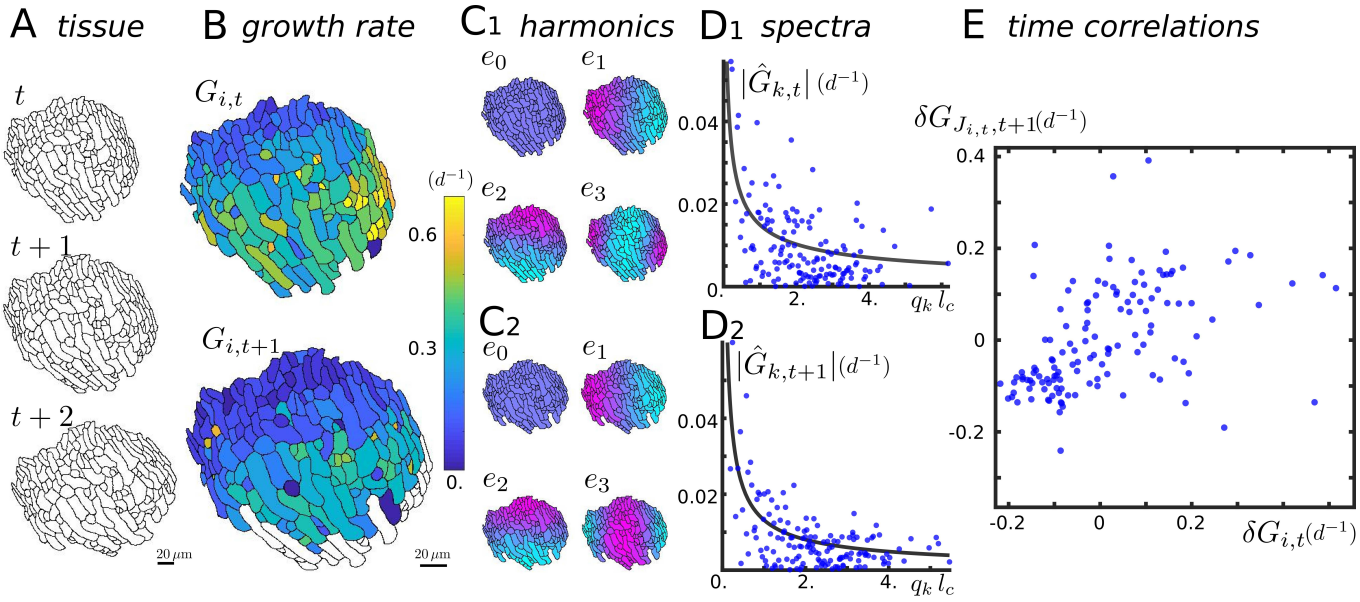

FIG. 2. Quantification of spatial and temporal fluctuations in cell growth. Day (d) is used as a unit of time. **A** Three snapshots of a plant tissue (abaxial sepal epidermis from wild-type plant) taken at one-day intervals. Black lines represent cell contours. **B** Heatmaps of relative areal growth rate between times t and $t+1$, $G_{i,t}$, and between $t+1$ and $t+2$, $G_{i,t+1}$ for cell $\#i$. A growth rate of $1d^{-1}$ corresponds to a relative increase of area of 100% in 1 day. Growth rate of white cells could not be computed because they were not imaged at $t+2$. **C$_1$-C$_2$** The first 4 harmonics e_k ($k = 0, 1, 2,$ and 3) of the Cellular Fourier Transform (CFT) of the tissue at t and $t+1$, represented by a cyan (low value) to magenta (high values) color scheme. The harmonics e_k generalise sinusoidal waves and can be used to decompose the growth fields $G_{i,t}$ and $G_{i,t+1}$ into their respective CFTs $\hat{G}_{k,t}$ and $\hat{G}_{k,t+1}$. **D$_1$-D$_2$** Fourier spectra (blue dots) correspond to the modulus $|\hat{G}_{k,t}|$ and $|\hat{G}_{k,t+1}|$ of the CFTs and are shown as function of the wavenumber q_k of the harmonics e_k. Wavenumbers were non-dimensionalised using mean cell size l_c. Spectra were fitted to a power-law (dashed line) of the form $\Delta G_t q_k^{-\alpha_t} \Big/ \left(\sum_k q_k^{-2\alpha_t}\right)^{1/2}$ in order to characterise each spectrum with two numbers (see text). Here we have $\alpha_t = 0.54 \pm 0.08$ ($\pm$ standard error),$\alpha_{t+1} = 0.71 \pm 0.08$, $\Delta G_t = 0.157 \pm 0.012\, d^{-1}$ and $\Delta G_{t=1} = 0.134 \pm 0.012\, d^{-1}$. **E** For temporal analyses, detrended areal growth rate was computed as the excess areal growth rate of a cell with respect to neighboring cells. Detrended growth $\delta G_{i,t+1}$ (excess cell growth between $t+1$ to day $t+2$) is plotted as a function of detrended growth rate $\delta G_{i,t}$ (excess cell growth beween t and $t+1$). Each blue dot corresponds to one cell that was followed from t to $t+2$. The degree of growth temporal correlation is quantified by the value of the Kendall correlation coefficient $\Gamma_t = 0.400 \pm 0.052$ ($\pm$ standard error). Two outliers were excluded from the plot to improve the readability of the figure.

to a spectrum scaling like $q^{-\alpha}$, with $\alpha = 1 - \beta/2$, as derived from our simplified model (see section Datasets and Methods). Although the limited range of wavenumbers did not allow us to test the power-law behavior, we used such power-laws, $\Delta G_t q_k^{-\alpha_t} \Big/ \left(\sum_k q_k^{-2\alpha_t}\right)^{1/2}$, to summarize the characteristics of a spectrum with two numbers: the amplitude, ΔG_t, and the exponent, α_t . The specific choice made for the form of the power law is such that, following the Parseval theorem, ΔG_t measures the standard deviation of growth while α_t measures its spatial correlations. We used statistical inference to estimate α_t and ΔG_t, which we found to approximately range 0.1 to 0.9 and 0.1 to $0.6\, d^{-1}$, respectively, over all sepals and time points considered.

We estimated temporal correlations of growth using correlation coefficients. We considered the correlations of relative areal cell growth $G_{i,t}$ from t to $t+1$ and $G_{J_{i,t},t+1}$ from $t+1$ to $t+2$, where the set $J_{i,t}$ in subscript contains the labels of all daughters of cell i at time $t+1$ and $G_{J_{i,t},t+1}$ is their areal growth rate, see section Datasets and Methods for details. To avoid any bias due to overall gradients in growth rate [19], we computed detrended cell growth $\delta G_{i,t}$ by substracting from each areal growth rate the average growth in the group of neighboring cells, see Supplementary information. The scatter plot in FIG.2**E** of $\delta G_{J_{i,t},t+1}$ as function of $\delta G_{i,t}$ illustrates the fact growth is persistent in time: For instance cells that grow more than their neighbors between t and $t+1$ tend to remain so between $t+1$ and $t+2$. We then computed Kendall's correlation coefficient , Γ_t, which is based on the rank of data and is less sensitive to outliers than the more classical Spearman correlation coefficient [26]. Over all sepals and time points considered, Γ_t approximately ranged -0.1 to 0.6.

We thus obtained a minimal set of parameters to describe growth fields and their fluctuations: average growth rate, $\overline{G}_t$, extent (exponent) of spatial correlations, α_t, amplitude of spatial correlations, ΔG_t, and temporal

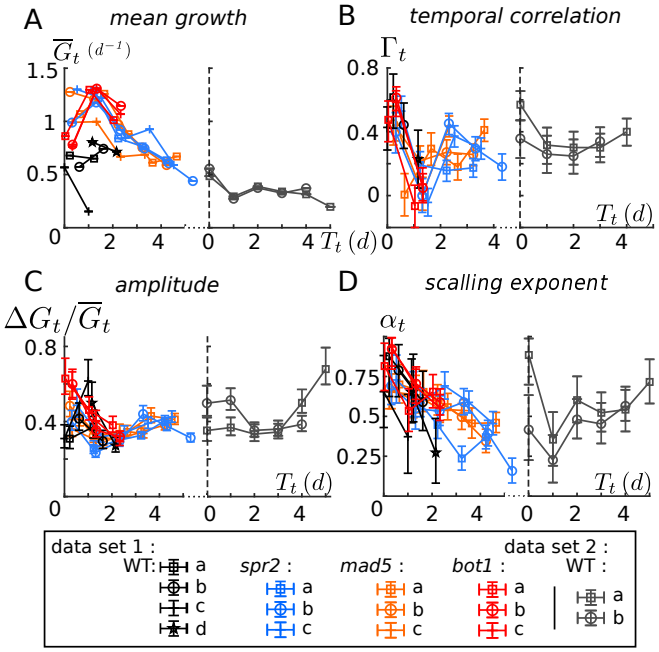

FIG. 3. Parameters that characterise growth fields in sepals from wild-type and mutant plants. The sequences were temporally aligned and parameters are shown as a function of the synchronized time T_t. **A** Growth rate averaged over the tissue $\overline{G}_t$. **B** Temporal correlation coefficient Γ_t. **C** Dimensionless amplitude of the Cellular Fourier Transform (CFT) $\Delta G_t/\overline{G}_t$. **D** Scaling exponent of the CFT α_t. The two datasets correspond to two slightly different culture conditions. Black, blue, orange and, red symbols/lines correspond respectively to wild-type, *spr2* mutant, *mad5* mutant, and *bot1* mutant from the first dataset, while gray symbols/lines corrrespond to wild-type plants from the second set. Error bars indicate the 90% confidence intervals.

correlation coefficient Γ_t. Next, we analysed differences and common features between sepals based on this minimal set of parameters.

Temporal and spatial correlations of cell growth vary across genotypes and culture conditions

We compared growth fluctuations between genotypes and culture conditions. As explained in the introduction, we chose to focus on mutants affected in responses to mechanical stress, *spiral2* (*spr2*) and *katanin* (*bot1* and *mad5*), in addition to wild-type plants. We analyzed sepals from 3 genotypes in 2 culture conditions and at different developmental stages. In order to enable the comparison of several sepals that were imaged starting from different stages, we temporally aligned live imaging sequences along a common time frame using sepal width, building upon the approach developed in [27], see Methods. The parameters that characterise growth fields in all these sequences are shown in FIG. 3. Despite variability within and between genotypes, a few trends can be seen over time: decreases of mean growth rate (panel **A**), approximate decrease of the relative amplitude of growth fluctuations (panel **C**), decrease of the extent of spatial correlations (panel **D**); temporal correlations seem however more erratic (panel **B**).

In order to quantify differences induced by mutations or culture conditions, we used wild-type plants from dataset 1 as a reference and we estimated the shift in growth parameters between the reference and other genotypes or condition, see FIG. 4. In practice we calculated this shift between pairs of sepals (one sepal from wild-type dataset 1 and one sepal from the other genotype/condition) over the common observation time points and then we computed the average shift over all sepal pairs, as well as the standard deviation of the shift. The change in culture conditions reduces average growth rate (panel **A**), temporal correlations (panel **B**), and extent of spatial correlations (panel **D**), leaving the amplitude of fluctuations unchanged (panel **C**). We found average growth $\overline{G}_t$ to be higher in mutants than in wild-type (panel **A**) over the temporal window considered. When comparing mutants to wild-type plants, temporal correlations are lower (panel **B**), while the extent of spatial correlations is higher (panel **D**). There is no clear conclusion for the amplitude of fluctuations, because the two *katanin* alleles (*bot1* and *mad5*) show different trends (panel **C**).

A conserved relation between growth parameters supports fluctuation stretching

Next, we sought relations between growth parameters that would hold across genotypes, data sets, and developmental stages. We first considered the pairwise relations between the growth parameters defined for each sepal: mean growth rate, $\overline{G}_t$, temporal correlation coefficient, Γ_t, normalised amplitude of spatial fluctuations, $\Delta G_t/\overline{G}_t$, and extent (exponent) of spatial fluctuations, α_t. The corresponding scatter plots are shown in FIG. 5.**A-F**. To assess these pairwise relations, we computed Kendall's correlation coefficient between the two parameters. We found rather weak trends overall. The strongest trends are between the exponent, α_t, and the temporal correlation coefficient, Γ_t, and between α_t and the average growth $\overline{G}_t$. Interestingly, these trends would be consistent with fluctuation stretching: larger spatial extent of fluctuations is favored by higher growth rate and by higher temporal persistence, see above. We therefore tested more directly the predictions from fluctuation stretching.

Fluctuation stretching does not reduce to a pairwise relation between growth parameters because it relates spatial correlations to time persistence and growth rate. If this phenomenon is at play in sepals, then Eq. 1 and $\alpha = 1 - \beta/2$ (see section Datasets and Methods) yield $\alpha_t = 1 - 2/(\tau_t \overline{G}_t)$, where τ_t is the persistence time. We could measure all parameters of this relation but τ_t. Nev-

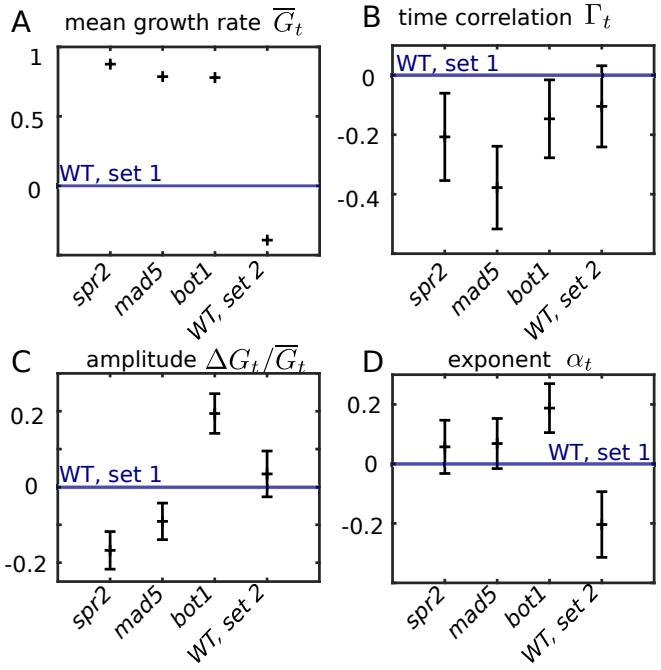

FIG. 4. Differences in growth parameters between mutant and wild-type (WT) sepals grown in same conditions or between wild-type sepals grown in distinct conditions. **A** Growth rate averaged over the sepal, $\overline{G}_t$. The error on $\overline{G}_t$ is smaller than the size of the crosses. **B** Temporal correlation coefficient, Γ_t. **C** Dimensionless amplitude of growth fluctuations, $\Delta G_t/\overline{G}_t$. **D** Exponent quantifying spatial extent of growth fluctuations, α_t. Wild-type from dataset 1 was used as a reference in all case. Symbols and errors bars correspond to the mean and standard deviation of the difference, respectively. Error bars correspond to standard deviations; they combine uncertainties of the two genotypes or culture conditions compared. Average growth parameters over all available reference data (WT dataset 1) were taken as reference units.

ertheless the temporal correlation coefficient, Γ_t, should be a decreasing function of $\Delta t/\tau_t$, $\Gamma_t = f(\Delta t/\tau_t)$, where $\Delta t = 1d$ is the time delay between two time steps of live imaging, because correlations between states of the sepal at consecutive time steps are higher if the time delay is small compared to the persistence time. As a consequence, we predict that

$$\Gamma_t = f\left(\Delta t\,\overline{G}_t(1-\alpha_t)/2\right).$$

We plotted in FIG. 5**G.** the time correlation coefficient Γ_t as a function of $\Delta t\,\overline{G}_t/2(1-\alpha_t)$. The trend is much clearer than in all other panels of FIG. 5 (Kendall's coefficient $\kappa = -0.48$) and the data seem to collapse along a line. We used statistical inference to perform a linear fit of the data, $\Gamma_t = \beta_0 + \beta_1 \Delta t \overline{G}_t(1-\alpha_t)/2$, see Supplementary information. We obtained fit parameters $\beta_0 = 0.596 \pm 0.024$ and $\beta_1 = -1.87 \pm 0.15$, with relatively small standard deviations. We then confirmed with a Kolmogorov-Smirnov test that the residuals (the spread of the data around the fit) could be explained by the uncertainty on the estimates of τ_t and Γ_t, see Supplemen-

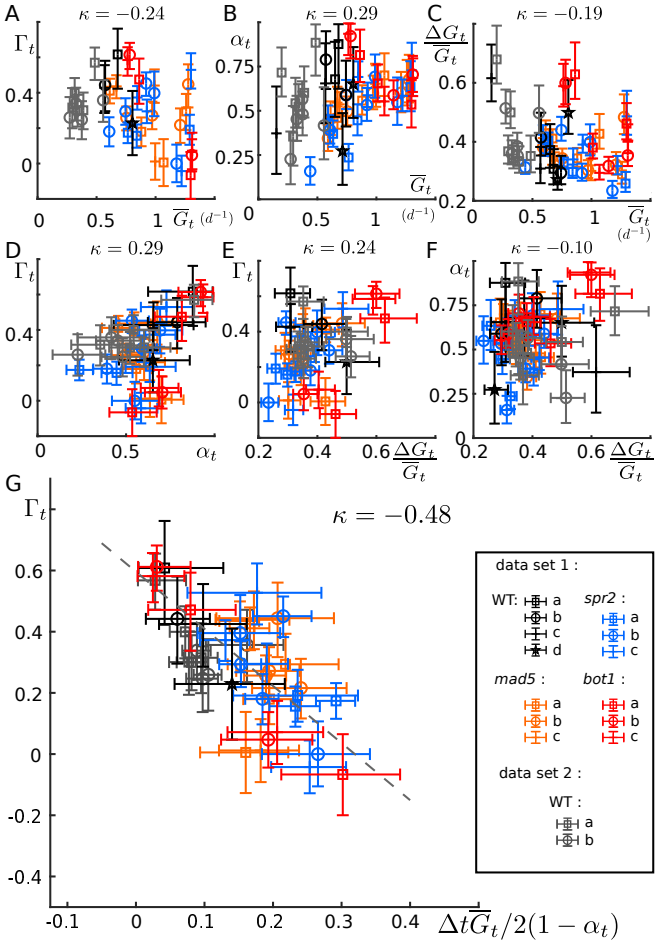

FIG. 5. Relations between parameters of growth (fluctuations). **A-F** Pairwise scatter plots of all growth parameters. **A-C** Temporal correlation coefficient Γ_t, exponent of spatial fluctuations α_t, and dimensionless amplitude of spatial fluctuations, $\Delta G_t/\overline{G}_t$, respectively, as function of average growth $\overline{G}_t$. **D-E** Temporal correlation coefficient, Γ_t, as function of exponent of spatial fluctuations, α_t, and dimensionless amplitude of spatial fluctuations, $\Delta G_t/\overline{G}_t$, respectively. **F** Exponent of spatial fluctuations, α_t, as function of their dimensionless amplitude, $\Delta G_t/\overline{G}_t$. **G** Test of the coupling between temporal and spatial fluctuations, as resulting from fluctuation stretching. Temporal correlation coefficient Γ_t as a function of the combination $\Delta t\overline{G}_t/2(1-\alpha_t)$ where $\Delta t = 1\,d$ is the time step of live imaging. The dashed line corresponds to a linear fit, $\Gamma_t = \beta_0 + \beta_1 \Delta t \overline{G}_t/2(1-\alpha_t)$, with fit parameters $\beta_0 = 0.596 \pm 0.024$ and $\beta_1 = -1.87 \pm 0.15$. The analysis of the fit residuals supports a deterministic relation between the two, see Supplementary Information. In all panels, error bars show the 90 % confidence intervals; black, blue, orange, and red symbols correspond to wild-type, *spr2*, *mad5* and *bot1* sepals from dataset 1, respectively, while gray symbols correspond to wild-type sepals from dataset 2. Kendall's correlation coefficient, κ, is shown above each plot.

tary Information, while the same analysis for the other plots (FIG.5**A-F**) confirmed that none of these plots was consistent with a linear behavior. Altogether these results support the hypothesis of a deterministic relation between Γ_t and $\Delta t\,\overline{G}_t/2(1-\alpha_t)$ and therefore indicate that fluctuation stretching is at play in growing sepals.

DISCUSSION

Our analysis provides evidence that growth stretches time persistent fluctuations: while no clear pairwise relation could be made among the different growth parameters, see FIG.5**A-F**, the clear trend of panel **G** suggest that the persistence time can be deduced from space correlations and tissue growth. This phenomenon explains why higher correlation among cells (higher spatial correlations) may induce more variable organ shape and size [13]. Fluctuation stretching gives a prominent role to the persistence time (correlation time) in controlling spatial correlations in the tissue. Any mechanism that would decrease persistence time would reduce spatial correlations and, as a consequence, variability of organ contours. Accordingly, reducing persistence time would yield robust morphogenesis.

Surprisingly, we found that the temporal correlation coefficient, Γ_t, is generally not much smaller than unity, implying that the persistence time, τ_t, is not much smaller than the time scale of growth $1/\overline{G}_t$. This might be specific to plants. The cell wall sets the local growth rate, and, at the same time, is remodelled at the pace of growth, so that the persistence time of fluctuations of cell wall properties is given by the time scale of growth. It would be worthwhile to extend our study to expanding animal tissues imaged live such as the imaginal disc of the fruit fly [28]. In animal tissues that undergo convergent extension, we would expect fluctuation stretching to operate only in the direction of extension, and so spatial correlations would be highly anisotropic.

We found a higher spatial extent of correlations (higher α_t) in mutant genotypes. This means that these mutants potentially have more variable shapes or are less robust to perturbations, consistent with the observation that the width of *bot1* and *mad5* sepals varies more with trichome number than WT plants [18]. Models predicted that variability of organ contours is minimal for a well-defined level of feedback from mechanical stress to cellulose synthesis [14], leading to the speculation that in wild-type sepals the level of mechanical feedback is optimised so as to reduce variability of sepal shape, compared to mutants with lower (*bot1*) or with higher (*mad5*) mechanical feedback. This level of mechanical feedback also corresponds to a minimum of the persistence time of fluctuations, τ, highlighting the importance of this time scale in setting the robustness of organ shape and size.

Fluctuation stretching is a kinematic phenomenon: properties of cells or of regions of cells are carried (advected) by tissue growth and deformation; the persistence time of these properties sets how they are carried to larger or smaller spatial scales, in the case of tissue expansion or tissue shrinkage, respectively. This kinematic phenomenon applies to any type of property or field as far as it is carried by tissue growth and deformation, such as protein concentrations in cells. Advection also applies to non-random properties, in line with theoretical models of polarity fields showing that a combination of morphogens, advection, and time persistence can reproduce the shapes of leaves [29], or with models of leaf vasculature that show that areole (region delimited by veins) shape is advected by leaf growth [30].

Altogether, our work sheds light on the role of persistence time, that is the memory of previous states of a given property, in the robustness of morphogenesis. The investigation of spatiotemporal fluctuations may provide a new avenue to characterize organ development.

AUTHORS CONTRIBUTIONS

Conceptualisation: AF, AB. Data curation: LH, AF. Investigation: AF. Methodology: AF. Writing – original draft: AF, AB. Writing – review and editing: all authors. Supervision: AR, CBL, AB. Funding acquisition: AR, CBL, AB.

ACKNOWLEDGMENT

We gratefully thank Nathan Hervieux and Olivier Hamant for providing the live imaging data used here. This work was supported by the Human Frontier Science Program grant no. RGP0008/2013 (A.B., A.H.K.R., C.-B.L.), by the US National Institutes of Health Institute of General Medicine grant no. R01 GM134037 (A.H.K.R.), by the US National Science Foundation grant no. MCB-2203275 (A.H.K.R.), by the Université de Lyon through the program "Investissements d'Avenir" grant no. ANR-11-IDEX-0007 (A.B.), and by the French National Research Agency grant no. ANR-21-CE30-0039-01 (A.B.).

DATASETS AND METHODS

Model for fluctuation stretching

We introduced a simple model for the dynamics of a quantity $\Phi(x,t)$ that varies with position vector, x, in D-dimensional Cartesian space and with time, t. We assumed Φ to be advected by tissue growth at rate $\overline{G}$, to have a persistence time τ, relaxing towards its reference value $\langle\Phi\rangle$, and to be driven by a stochastic source $\xi(x,t)$, so that

$$\partial_t\Phi(x,t)+\overline{G}/D\,x\cdot\partial_x\Phi(x,t) = -(\Phi(x,t)-\langle\Phi\rangle)/\tau+\xi(x,t). \quad (2)$$

This equation can be solved as shown in the Supplementary note. We obtained the deviation $\Delta\Phi(x,t) = \Phi(x,t) - \langle\Phi\rangle$,

$$\Delta\Phi(x,t) = e^{-t/\tau}\Delta\Phi(x\,e^{-t\,\overline{G}/D},0) + \int_0^t \frac{ds}{\tau} e^{-(t-s)/\tau}\xi(x\,e^{-(t-s)\,\overline{G}/D},s). \quad (3)$$

In the absence of noise, this equation corresponds to the plots in FIG.1.**A**: the lengthscales of variation of the initial pattern are enlarged of a factor $e^{t\,\overline{G}/D}$, while the amplitude of the pattern decays like $e^{-t/\tau}$. We then assumed the noise to be Gaussian, with $\langle\xi(x,t)\rangle = 0$ and $\langle\xi(x,t)\xi(x+\ell,t+s)\rangle = K\delta(s)g(|\ell|)$, where $\langle.\rangle$ stands for an ensemble average, $\delta(.)$ is the Dirac distribution, and $g(|\ell|)$ is a function that vanishes when $\ell \to \pm\infty$. In the Supplementary note, we found the spatial correlation function $C(l) = \langle\Delta\Phi(x,t)\Delta\Phi(x+l,t)\rangle/\langle|\Delta\Phi(x,t)|^2\rangle$ to take the form

$$C(l) = |l|^{-2D/(\tau\overline{G})} f(|l|), \quad (4)$$

where $f(|l|) = \int_0^{|l|} du\, u^{2D/(\tau\overline{G})-1} g(u)$. $C(l)$ exhibit a long tail with an exponent $\beta = 2D/(\tau\overline{G})$, proving Eq.1. Finally, we considered the Fourier transform $\hat{\Phi}(q,t) = \int dx e^{-Iq\cdot x}\Phi(x,t)$ and predicted the root mean squared spectrum $\langle\hat{\Phi}^2(q,t)\rangle^{1/2}$ to behave as a power law $\propto |q|^{-\alpha}$ with

$$\alpha = D/2 - \beta/2 = D/2 - D/(\tau\overline{G}). \quad (5)$$

We can therefore estimate spatial correlations in using the Fourier spectrum and test the existence of fluctuation stretching based on this last equation.

Experimental datasets

In order to reliably analyse fluctuations of growth rate, we chose datasets of sepals imaged with the highest spatial resolution possible among those published. We used live imaging sequences from [19] (dataset 1) and from [18] (dataset 2). Voxel size was $0.12 \times 0.12 \times 0.50\,\mu m^3$. All plant lines in these sequences were crosses between Ws-4 and Col-0 ecotypes, harbouring respectively the microtubule reporter *p35S::GFP-MBD* and the membrane reporter *pUQ10::Lti6b-2xmCherry* [19]. The two datasets had different culture conditions (type of lighting). Dataset 1 contained wild-type plants, the *spr2-2* allele of *SPIRAL2* that was originally obtained in a Col-0 background, the *bot1-7* allele of *Katanin* that was originally obtained in a Ws-4 background, and the *mad5* allele of *Katanin* that was originally obtained in a Col-0 background (unpublished sequences obtained in parallel with those from [19]).

Segmentation

For sepals not already processed in [18, 19], cells of the abaxial epidermis were segmented and tracked in time using MorphoGraphX [31]. A triangular mesh was obtained for the outer organ surface in which cells were identified and well delimited.

Computation of growth rates

We aimed at analysing fluctuations of cell relative areal growth rates tangentially to the sepal and therefore to get rid of the curvature of the outer surface of cells. To do so, we redefined the surface of cells from the linear interpolation of their contours. Areal growth rate was defined from the cell surface area at successive time steps. At time t, each cell is labeled by an index i and has surface area $S_{i,t}$. Cell i may divide between t and $t+1$; the set $J_{i,t}$ contains the labels of all daughters of cell i at time $t+1$ ($J_{i,t}$ is reduced to a single label if cell i has not divided). We only consider cells which or whose daugthers remain in the segmented region from t to $t+1$. The areal growth rate of the cell i at a time t is then defined as

$$G_{i,t} = \Big(\sum_{j\in J_{i,t}} S_{j,t+1}\Big)/S_{i,t} - 1. \quad (6)$$

Tissular growth is in turn defined as $\overline{G}_t = (\sum_i \sum_{j\in J_{i,t}} S_{j,t+1})/(\sum_i S_{i,t}) - 1$.

Cellular Fourier Transforms

The Fourier harmonics are built from a coarse and discreet version of the Laplace operator. To compute this operator we triangularized cell surfaces using the 'MESH2D' matlab algorithm [32, 33]. More details can be found in the Supplementary Information. The Cellular Fourier Transform (CFT) $\hat{G}_{k,t}$ of cell relative areal growth gives the weights by which growth is decomposed over the harmonics e_k of the CFT. In this paper, the definition of the CFT differ from the one in [25] by a prefactor $1/\sqrt{S_t}$ where S_t is the total surface area. This change simplifies the interpretation of Fourier spectra: the coefficients have the same physical dimension as the

original signal and the first coefficient is the average of the signal.

Scaling exponent and amplitude of fluctuations

We quantified spatial correlations in the tissue by fitting the spectral density with a power law. To do so, we assumed a Gaussian distribution for the CFT, centred around 0 with a standard deviation verifying,

$$\sigma_{k,t} = \Delta G_t q_k^{-\alpha_t} / \sqrt{\sum_l q_l^{-2\alpha_t}} \tag{7}$$

where ΔG_t and the scaling exponent α_t are the fit parameters characterizing respectively the amplitude and the extent of spatial correlation of growth fluctuations. For the fit, we used statistical inference as detailed in the Supplementary Information. Doing so, we estimated a probability for the parameters ΔG_t and α_t, their expected value, their standard error, and median values. We also estimated the 90% confidence interval, from the fifth to the ninety fifth percentiles.

Temporal correlations

We estimated temporal correlations of relative areal growth in considering cell growth $G_{i,t}$ from t to $t+1$ and cells growth $G_{J_{i,t},t+1}$ from $t+1$ to $t+2$. $G_{J_{i,t},t+1}$ is simply the areal growth rate from t to $t+1$ of the descendants of the cell i in the segmentation at t:

$$G_{J_{i,t},t+1} = \frac{\sum_{j\in J_{i,t}} \sum_{l\in J_{j,t+1}} S_{l,t+2}}{\sum_{j\in J_{i,t}} S_{j,t+1}} - 1. \tag{8}$$

To avoid any bias due to systematic variation of growth at organ scale [19], we used the detrended cell growth $\delta G_{i,t}$, which can be defined by subtracting average growth in a neighborhood to cell growth, see Supplementary Information. Temporal correlations were computed as Kendall's correlation coefficient Γ_t of $\delta G_{i,t}$ and $\delta G_{J_{i,t},t+1}$. Kendall's correlation coefficient is rank-based and so is less sensitive to outliers [26]. We used boostrapping to obtain confidence intervals and uncertainties.

We note that Γ_t tends to be underestimated: A positive error on $S_{J_{i,t},t+1}$ leads to an overestimation of $\delta G_{i,t}$ and an underestimation of $\delta G_{J_{i,t},t+1}$, inducing a negative correlation between $\delta G_{i,t}$ and $\delta G_{J_{i,t},t+1}$. This may explain the few negative values of Γ_t. We found this negative bias to be stronger when we defined growth from the cells outer surface area, leading us to use the interpolation of cell contours instead (see above).

Comparing genotypes

To describe the impact of mutations on growth parameters, we compared tissues at equivalent developmental stages. We first synchronized all the live imaging sequences from a dataset by considering the time curves of organ widths for every considered tissues and finding the time delays ensuring their superposition, building upon the approach developed in [27], leading to a corrected time T_t. We defined the mean shift of a quantity Φ_t as

$$D = \frac{\sum_{n',t'} \sum_{n,t} W_{t't}^{(n',n)} (\Phi_{t'}^{(n')} - \Phi_t^{(n)})}{\sum_{n',t'} \sum_{n,t} W_{t't}^{(n',n)}}, \tag{9}$$

where the upper exponents (n') and (n) label the pair of conditions compared (e.g. one mutant and the reference wild-type). The sums $\sum_{n',t'}$ and $\sum_{n,t}$ are over all squences of the mutant and the WT respectively. D quantifies how much, in average, the quantities Φ_t for the mutants are shifted from the WT where $W_{t',t}^{(n',n)}$ gives the weights at which each pair is considered. A weight differs from 0 only if the values of synchronized times T_t of the pair are close, see Supplementary Information for details.

[1] Lilan Hong, Mathilde Dumond, Mingyuan Zhu, Satoru Tsugawa, Chun-Biu Li, Arezki Boudaoud, Olivier Hamant, and Adrienne HK Roeder. Heterogeneity and robustness in plant morphogenesis: from cells to organs. *Annual review of plant biology*, 69:469–495, 2018.

[2] Deb Sankar Banerjee, Akankshi Munjal, Thomas Lecuit, and Madan Rao. Actomyosin pulsation and flows in an active elastomer with turnover and network remodeling. *Nature Communications*, 8(1):1121, 2017.

[3] Yuchen Long, Ibrahim Cheddadi, Gabriella Mosca, Vincent Mirabet, Mathilde Dumond, Annamaria Kiss, Jan Traas, Christophe Godin, and Arezki Boudaoud. Cellular heterogeneity in pressure and growth emerges from tissue topology and geometry. *Current Biology*, 30(8):1504–1516, 2020.

[4] Shahaf Armon, Michael Moshe, and Eran Sharon. The multiscale nature of leaf growth fields. *Communications Physics*, 4(1):1–7, 2021.

[5] Jonathan R Chubb. Symmetry breaking in development and stochastic gene expression. *Wiley Interdisciplinary Reviews: Developmental Biology*, 6(6), 2017.

[6] Francis Corson, Lydie Couturier, Hervé Rouault, Khalil Mazouni, and François Schweisguth. Self-organized notch dynamics generate stereotyped sensory organ patterns in drosophila. *Science*, 356(6337):eaai7407, 2017.

[7] Bruno Moulia, Stéphane Douady, and Olivier Hamant. Fluctuations shape plants through proprioception. *Science*, 372(6540), 2021.

[8] Kenneth D Irvine and Boris I Shraiman. Mechanical control of growth: ideas, facts and challenges. *Development*, 144(23):4238–4248, 2017.

[9] Vincent Mirabet, Pradeep Das, Arezki Boudaoud, and Olivier Hamant. The role of mechanical forces in plant morphogenesis. *Annual review of plant biology*, 62:365–385, 2011.

[10] Guo-Jie Jason Gao, Michael C Holcomb, Jeffrey H Thomas, and Jerzy Blawzdziewicz. Embryo as an active granular fluid: stress-coordinated cellular constriction chains. *Journal of Physics: Condensed Matter*, 28(41):414021, 2016.

[11] David R Hipfner and Stephen M Cohen. Connecting proliferation and apoptosis in development and disease. *Nature Reviews Molecular Cell Biology*, 5(10):805, 2004.

[12] Marco Milán, Sonsoles Campuzano, and Antonio García-Bellido. Cell cycling and patterned cell proliferation in the wing primordium of drosophila. *Proceedings of the National Academy of Sciences*, 93(2):640–645, 1996.

[13] Lilan Hong, Mathilde Dumond, Satoru Tsugawa, Aleksandra Sapala, Anne-Lise Routier-Kierzkowska, Yong Zhou, Catherine Chen, Annamaria Kiss, Mingyuan Zhu, Olivier Hamant, et al. Variable cell growth yields reproducible organ development through spatiotemporal averaging. *Developmental cell*, 38(1):15–32, 2016.

[14] Antoine Fruleux and Arezki Boudaoud. Modulation of tissue growth heterogeneity by responses to mechanical stress. *Proceedings of the National Academy of Sciences*, 116(6):1940–1945, 2019.

[15] Ojan Khatib Damavandi and David K Lubensky. Statistics of noisy growth with mechanical feedback in elastic tissues. *Proceedings of the National Academy of Sciences*, 116(12):5350–5355, 2019.

[16] Wentian Li. Expansion-modification systems: a model for spatial 1/f spectra. *Physical Review A*, 43(10):5240, 1991.

[17] Andrew R Liddle and David H Lyth. *Cosmological inflation and large-scale structure*. Cambridge university press, 2000.

[18] Nathan Hervieux, Satoru Tsugawa, Antoine Fruleux, Mathilde Dumond, Anne-Lise Routier-Kierzkowska, Tamiki Komatsuzaki, Arezki Boudaoud, John C Larkin, Richard S Smith, Chun-Biu Li, et al. Mechanical shielding of rapidly growing cells buffers growth heterogeneity and contributes to organ shape reproducibility. *Current Biology*, 27(22):3468–3479, 2017.

[19] Nathan Hervieux, Mathilde Dumond, Aleksandra Sapala, Anne-Lise Routier-Kierzkowska, Daniel Kierzkowski, Adrienne HK Roeder, Richard S Smith, Arezki Boudaoud, and Olivier Hamant. A mechanical feedback restricts sepal growth and shape in arabidopsis. *Current Biology*, 26(8):1019–1028, 2016.

[20] Masayoshi Nakamura, Jelmer J Lindeboom, Marco Saltini, Bela M Mulder, and David W Ehrhardt. Spr2 protects minus ends to promote severing and reorientation of plant cortical microtubule arrays. *Journal of Cell Biology*, 217(3):915–927, 2018.

[21] Magalie Uyttewaal, Agata Burian, Karen Alim, Benoît Landrein, Dorota Borowska-Wykręt, Annick Dedieu, Alexis Peaucelle, Michał Ludynia, Jan Traas, Arezki Boudaoud, et al. Mechanical stress acts via katanin to amplify differences in growth rate between adjacent cells in arabidopsis. *Cell*, 149(2):439–451, 2012.

[22] Olivier Hamant, Marcus G Heisler, Henrik Jönsson, Pawel Krupinski, Magalie Uyttewaal, Plamen Bokov, Francis Corson, Patrik Sahlin, Arezki Boudaoud, Elliot M Meyerowitz, et al. Developmental patterning by mechanical signals in arabidopsis. *science*, 322(5908):1650–1655, 2008.

[23] Arun Sampathkumar, Pawel Krupinski, Raymond Wightman, Pascale Milani, Alexandre Berquand, Arezki Boudaoud, Olivier Hamant, Henrik Jönsson, and Elliot M Meyerowitz. Subcellular and supracellular mechanical stress prescribes cytoskeleton behavior in Arabidopsis cotyledon pavement cells. *eLife*, 3:e01967, 2014.

[24] Alexander R Paredez, Christopher R Somerville, and David W Ehrhardt. Visualization of cellulose synthase demonstrates functional association with microtubules. *Science*, 312(5779):1491–1495, 2006.

[25] Antoine Fruleux and Arezki Boudaoud. Cellular fourier analysis for geometrically disordered materials. *Physical Review Research*, 3(2):023036, 2021.

[26] Christophe Croux and Catherine Dehon. Influence functions of the spearman and kendall correlation measures. *Statistical methods & applications*, 19(4):497–515, 2010.

[27] Corentin Mollier, Joanna Skrzydeł, Dorota Borowska-Wykręt, Mateusz Majda, Vincent Bayle, Virginie Battu, Jean-Chrisologue Totozafy, Mateusz Dulski, Antoine Fruleux, Roman Wrzalik, Grégory Mouille, Richard S. Smith, Françoise Monéger, Dorota Kwiatkowska, and Arezki Boudaoud. Spatial consistency of cell growth direction during organ morphogenesis requires CELLULOSE SYNTHASE INTERACTIVE1. *Cell Reports*, 42(7):112689, July 2023.

[28] Silvia Aldaz, Luis M Escudero, and Matthew Freeman. Live imaging of Drosophila imaginal disc development. *Proceedings Of The National Academy Of Sciences Of The United States Of America*, 107(32):14217 – 14222, August 2010.

[29] Erika E Kuchen, Samantha Fox, Pierre Barbier De Reuille, Richard Kennaway, Sandra Bensmihen, Jerome Avondo, Grant M Calder, Paul Southam, Sarah Robinson, Andrew Bangham, et al. Generation of leaf shape through early patterns of growth and tissue polarity. *Science*, 335(6072):1092–1096, 2012.

[30] Yohai Bar-Sinai, Jean-Daniel Julien, Eran Sharon, Shahaf Armon, Naomi Nakayama, Mokhtar Adda-Bedia, and Arezki Boudaoud. Mechanical Stress Induces Remodeling of Vascular Networks in Growing Leaves. *PLOS Computational Biology*, 12(4):e1004819, April 2016.

[31] Pierre Barbier de Reuille, Anne-Lise Routier-Kierzkowska, Daniel Kierzkowski, George W Bassel, Thierry Schüpbach, Gerardo Tauriello, Namrata Bajpai, Sören Strauss, Alain Weber, Annamaria Kiss, et al. Morphographx: A platform for quantifying morphogenesis in 4d. *Elife*, 4:e05864, 2015.

[32] D Engwirda. Unstructured mesh methods for the navier-stokes equations. *Undergraduate Thesis, School of Engineering, University of Sidney*, 2005.

[33] Darren Engwirda. Locally optimal delaunay-refinement and optimisation-based mesh generation. 2014.

Supplementary note

—

Growth couples temporal and spatial fluctuations of tissue properties during morphogenesis

Antoine Fruleux*
RDP, Université de Lyon, ENS de Lyon, UCB Lyon 1, INRAE, CNRS, 69364 Lyon Cedex 07, France
LadHyX, CNRS, Ecole polytechnique, Institut Polytechnique de Paris, 91128 Palaiseau Cedex, France and
LPTMS, CNRS, Université Paris-Saclay, 91405, Orsay, France.

Lilan Hong
Institute of Nuclear Agricultural Sciences, Key Laboratory of Nuclear Agricultural Sciences of Ministry of Agriculture and Zhejiang Province, College of Agriculture and Biotechnology, Zhejiang University, Hangzhou, China.

Adrienne H. K. Roeder
Weill Institute for Cell and Molecular Biology and Section of Plant Biology, School of Integrative Plant Science; Cornell University, Ithaca, New York 14853, USA

Chun-Biu Li
Department of Mathematics, Stockholm University, 106 91 Stockholm, Sweden

Arezki Boudaoud†
RDP, Université de Lyon, ENS de Lyon, UCB Lyon 1, INRAE, CNRS, 69364 Lyon Cedex 07, France and
LadHyX, CNRS, Ecole polytechnique, Institut Polytechnique de Paris, 91128 Palaiseau Cedex, France

(Dated: October 20, 2023)

I. MODEL FOR FLUCTUATION STRETCHING

A. Model

To support the explanation of fluctuation stretching proposed in FIG.1., we model the dynamics of a quantity Φ advected in a growing medium. If the medium grows isotropically and uniformly, its strain rate tensor in the D-dimensional space is $\overline{G}/D\delta_{ij}$ where $\overline{G}$ is the line, surface or volume growth for $D = 1$, 2, or 3 respectively and δ_{ij} is the Kronecker delta tensor. We assume the dynamics of the quantity Φ to be ruled by intrinsic cellular processes among which some are stochastic. For simplicity, we restrict our model to low order and linear dynamical systems. Denoting time by t and the Cartesian space coordinate vector by x, we assume the evolution of $\Phi(x,t)$ to be given by,

$$\partial_t\Phi(x,t) + \overline{G}/D\, x\cdot\partial_x\Phi(x,t) = -(\Phi(x,t) - \langle\Phi\rangle)/\tau + \xi(x,t), \tag{1}$$

where the material point at $x = 0$ serves as the origin of the spatial coordinate system. ∂_t and ∂_x respectively stand for the partial derivative with respect to time and for the gradient. The left hand side of (1) corresponds to the material time derivative. The first term in the right hand side ensures the relaxation of Φ toward its reference value $\langle\Phi\rangle$, while the second term accounts for stochasticity through the noise ξ.

* antoine.fruleux@universite-paris-saclay.fr

† arezki.boudaoud@polytechnique.edu

B. Linear response

We denote the deviation of Φ from its reference value by $\Delta\Phi(x,t) = \Phi(x,t) - \langle\Phi\rangle$. The persistence time τ sets the memory of the system as can be seen in the explicit solution of (1),

$$\Delta\Phi(x,t) = e^{-t/\tau}\Delta\Phi(x\,e^{-t\,\overline{G}/D},0) + \int_0^t \frac{ds}{\tau} e^{-(t-s)/\tau}\xi(x\,e^{-(t-s)\,\overline{G}/D},s). \tag{2}$$

In this equation, τ sets the time over which initial conditions persist and the delay over which the noise impacts the value of Φ.

C. Spatial correlation function

To describe the statistical properties of Φ, we assume the noise to be Gaussian, with $\langle\xi(x,t)\rangle = 0$ and $\langle\xi(x,t)\xi(x+l,t+s)\rangle = K\delta(s)g(|l|)$. $\langle.\rangle$ stands for an ensemble average. K is the noise strength. $\delta(.)$ is the Dirac distribution. The function $g(l) = \langle\xi(x,t)\xi(x+l,t)\rangle/\langle|\xi(x,t)|^2\rangle$ describes the spatial correlation of ξ, assumed to be regular and to vanish at infinity. The correlations of Φ can be computed using (2) with $t = -\infty$ as initial time. The space correlation function $C(l) = \langle\Delta\Phi(x,t)\Delta\Phi(x+l,t)\rangle/\langle|\Delta\Phi(x,t)|^2\rangle$ can then be written as,

$$C(l) = \int_0^{+\infty} (2\,ds/\tau)\, e^{-2\,s/\tau} g(|l|\, e^{-s\,\overline{G}/D}). \tag{3}$$

The space correlation function $C(l)$ is obtained by stretching the variation lengthscales of g by a factor ${}^{s\,\overline{G}/D}$ and summing the stretched functions with weights $e^{-2\,s/\tau}$. Changing the integration variable, we rewrite (3) as,

$$C(l) = |l|^{-2D/(\tau\overline{G})} f(|l|), \tag{4}$$

where the increasing function $f(|l|) = \int_0^{|l|} du\, u^{2D/(\tau\overline{G})-1} g(u)$ is expected to reach an asymptotic value as $|l|$ is large compared to the correlation length of ξ. (4) makes therefore explicit the long ranged property of C, characterized by the scaling exponent $\beta = 2D/(\tau\overline{G})$.

D. Fourier spectrum

The Fourier transform $\hat{\Phi}(q,t) = \int dx e^{-Iq\cdot x}\Phi(x,t)$ can be used to estimate the space correlation function $C(l)$. More exactly, the mean squared spectrum $\langle|\hat{\Phi}(q,t)|^2\rangle$ is proportional to the Fourier transform $\hat{C}(q) = \int dl e^{-Iq\cdot l}C(l) = |q|^{\beta-D}h(|q|)$ with $h(|q|) = \int d^D u|u|^{-\beta}f(|u|/|q|)e^{Iu\cdot\hat{y}}$ and $\hat{y}$ a unit vector. It exhibits a singularity for $|q| \to 0$ where it scales like $|q|^{-2\alpha}$, with

$$\alpha = D/2 - \beta/2 = D/2 - D/(\tau\overline{G}). \tag{5}$$

If the correlation length of the noise source is small, the root mean squared spectrum can be approximated by a power law whose amplitude relate to the standard deviation through the Parseval theorem and whose exponent α is given by the persistence time τ and growth rate $\overline{G}$ according to (5).

II. CELLULAR FOURIER TRANSFORM

Here we present the computation of cell surface area, we define the discrete Laplace operator, we explain how we built the Fourier harmonics based on this Laplace operator, and finally we define the Cellular Fourier Transform (CFT). The theoretical basis of the CFT may be found in [1].

A. Cell area and discrete Laplace operator

We compute cell area from the linear interpolation of cell contour. More precisely, we project the contour on a plane that is perpendicular to the surface vector. The contour being polygonal, the surface factor can be written

$1/2\sum_n \vec{r}_n \wedge \vec{r}_{n+1}$ where the sum is over the contour vertexes, $\vec{r}_n$ is their position, n indexes the position around the contour and $\wedge$ is the exterior product. We then triangulate the surface enclosed in the projected contour using the MESH2D Matlab package [2, 3]. To obtain a 3D mesh and determine the position of the mesh along the surface vector, we did a linear interpolation of the cell contours. The area $S_{i,t}$ for cell i at time t is then computed as the sum of areas of triangles in the triangulation, $S_{i,t} = \sum_m^{(i,t)} dS_m$, where m spans triangles of cell i at time t and dS_m is the area of triangle $\#m$. The tissue is made of N cells that are followed from t to $t+1$.

The discrete Laplace operator is a square matrix of size $N \times N$ and its components are given by

$$\bar{L}_{ij,t} = \delta_{ij} - \bar{W}_{ij,t}, \text{ with, } \bar{W}_{ij,t} = \sqrt{\frac{S_{i,t}}{S_{j,t}}} \frac{\sum_m^{(i,t)} dS_m \sum_n^{(j,t)} dS_n \exp(-d_{mn}/(5\,\ell_c))}{\sum_m^{(i,t)} dS_m \sum_j \sum_n^{(j,t)} dS_n \exp(-d_{mn}/(5\,\ell_c))}, \tag{6}$$

where indices $i = 0, 1, ..N-1$ and $j = 0, 1, ..N-1$ span the N cells of the tissue. d_{mn} is the distance between triangle m from cell i and triangle n from cell j, both considered at time step t. The unit of length is mean cell size $\ell_c = \sqrt{S_t/N}$, where S_t is the surface of the tissue at time t and N is the number of cells. Here we took the width $5l_c$ for the coarse Laplace operator.

B. Fourier harmonics

We start from the singular value decomposition of the Laplace operator $\bar{L}$, which yields left singular vectors V, right singular vectors U, and the singular values $\hat{L}_k$:

$$\bar{L}_{ij,t} = \sum_{k=0}^{N-1} \hat{L}_k\, V_{ki} U_{kj}. \tag{7}$$

The value taken by the k^{th}-harmonic in cell i at time step t is $1/S_{i,t}U_{ki}$. The wave number of the k^{th} harmonic is given by $q_k = 1/5\, Q(\hat{L}_k)$, with $Q(l) = \sqrt{(1-l)^{-2/3} - 1}$. The harmonics are indexed so that their index grows with the wave number.

C. Calculation of the CFT of cell growth

The areal growth rate of cell i at time step t is defined as $G_{i,t} = \left(\left(\sum_{j\in J_{i,t}} S_{j,t+1}\right)/S_{i,t} - 1\right)/\Delta t$ where $J_{i,t}$ is either the new label of cell i at time $t+1$ or the set of labels of the daughters of cell i if it has divided, while the time step is always $\Delta t = 1d$. The k^{th} CFT coefficient is then $\hat{G}_{k,t} = \sum_i U_{ki} G_{i,t} \sqrt{S_{i,t}/S_t}$ where S_t is the total area $S_t = \sum_i S_{i,t}$. Here we use a convention that differs from [1] by a multiplicative factor $1/\sqrt{S_t}$ in the definition of the CFT. This makes the interpretation of CFTs simpler: they have the same dimensions (units) as the original signal (here growth) and the first coefficient is equal to the average signal.

III. SPATIAL CORRELATIONS

We estimated spatial correlations of growth from the Fourier spectra *i.e.* from the distribution of Fourier transforms $\hat{G}_{k,t}$ and associated wavenumbers q_k. For this we used Bayesian inference.

A. Inference methods applied to Fourier spectra

To quantify spatial correlations, we assumed the CFT coefficients, $\hat{G}_{k,t}$ for $k \geq 2$, to be independent random Gaussian variables whose mean squared deviation follows a power law with respect to the wave number q_k,

$$\sigma_{k,t} = \Delta G_t^2 q_k^{-2\,\alpha_t} / \left(\sum_{l=2}^{N-1} q_l^{-2\,\alpha_t}\right), \tag{8}$$

the parameters ΔG_t and α_t quantifying the amplitude of growth fluctuations and their space correlations respectively. We make the choice not to consider the two first CFTs to avoid potential bias related to large scale growth

patterns, which should not be considered as fluctuations. For the derivation of the equations, it is more convenient to rewrite (8) as $\sigma_{k,t} = Q_k^{-2\,\alpha_t}/\xi$, where $Q_k = q_k/(\prod_{l=2}^{N-1} q_l)^{1/(N-2)}$ and $\xi = \sum_{k=2}^{N-1} Q_k^{-2\,\alpha_t}/(2\Delta G_t^2)$. We write the probability distribution fucntion of $\hat{G}_{k,t}$ as

$$p_k(\hat{G}|\xi,\alpha_t) = e^{-\xi \hat{G}^2 Q_k^{2\,\alpha_t}} \sqrt{\frac{\xi Q_k^{2\,\alpha_t}}{\pi}}. \tag{9}$$

We use Bayesian inference to estimate ξ and α_t, assuming a flat prior distribution for $\xi \in [0, +\infty[$ and $\alpha_t \in [0,1]$, which are the relevant range of parameters for (9). The posterior distribution for ξ and α_t takes the form

$$\mathcal{P}_{\Xi,A}(\xi,\alpha_t) = \frac{\prod_{k=2}^{N-1} p_k(\hat{G}_k|\xi,\alpha_t)}{\int_0^{+\infty} d\xi' \int_0^1 d\alpha \prod_{l=2}^{N-1} p_l(\hat{G}_l|\xi',\alpha)}. \tag{10}$$

We then substitute the probabilities p_k by their explicit form, noting that, by construction, $\prod_{k=2}^{N-1} Q_k = 1$, and computing the first integral in the denominator, we get

$$\mathcal{P}_{\Xi,A}(\xi,\alpha_t) = \frac{e^{-\xi \sum_{k=2}^{N-1} \hat{G}_{k,t}^2 Q_k^{2\,\alpha_t}}}{\xi\,\Gamma(N/2) \int_0^1 d\alpha (\xi \sum_{k=2}^{N-1} \hat{G}_{k,t}^2 Q_k^{2\alpha})^{-N/2}}, \tag{11}$$

where Γ is the Euler's gamma function.

B. Estimating amplitude of fluctuations and exponent of spatial correlations

To estimate ΔG_t, α_t and their uncertainty, we consider the joint cumulative distribution function $\mathcal{F}(\Delta G, \alpha)$, of having ΔG_t and α_t smaller than the values ΔG and α, respectively. This function can be written in terms of $\mathcal{P}(\xi,\alpha)$ as

$$\mathcal{F}(\Delta G, \alpha) = \int_0^{\alpha} d\alpha' \int_{\sum_{k=2}^{N-1} Q_k^{-2\,\alpha'}/(2\Delta G^2)}^{+\infty} d\xi\, \mathcal{P}(\xi,\alpha'). \tag{12}$$

By using the expression $\mathcal{P}(\xi,\alpha)$ in (11) and computing the second integral, we then get

$$\mathcal{F}(\Delta G, \alpha) = \frac{\int_0^{\alpha} d\alpha' \,(\sum_{k=2}^{N-1} \hat{G}_{k,t}^2 Q_k^{2\,\alpha'})^{-N/2} \Gamma\Big(N/2, \sum_{k=2}^{N-1} \frac{\hat{G}_{k,t}^2}{2\Delta G^2 q_k^{-2\,\alpha'}/\sum_{l=2}^{N-1} q_l^{-2\,\alpha'}}\Big)}{\int_0^1 d\alpha'' \,(\sum_{k=2}^{N-1} \hat{G}_{k,t}^2 Q_k^{2\,\alpha''})^{-N/2} \Gamma\Big(N/2\Big)}, \tag{13}$$

where $\Gamma(a,z) = \int_z^{+\infty} dt\, t^{a-1} e^{-t}$ is the incomplete gamma function.

We used the median as a representative value of the different quantities we considered. We estimate ΔG_t from the median $\mathcal{F}(\Delta G_t, 2) = .5$ and the 90% confidence interval $[\Delta G_{1,t}, \Delta G_{2,t}]$ from the 5^{th}, $\mathcal{F}(\Delta G_{1,t}, 2) = .05$, and the 95^{th} percentile, $\mathcal{F}(\Delta G_{2,t}, 2) = .95$. Similarly, we estimate α_t from the median $\mathcal{F}(+\infty, \alpha_t) = .5$ and the 90% confidence interval $[\alpha_{1,t}, \alpha_{2,t}]$ from the 5^{th}, $\mathcal{F}(+\infty, \alpha_{1,t}) = .05$, and the 95^{th} percentile, $\mathcal{F}(+\infty, \alpha_{2,t}) = .95$.

When we approximated their distributions by Gaussians (for fits or to estimate shifts from WT to mutants tissues), we used the the expected value and the standard deviations of α_t and ΔG_t. We estimated the expected value of α_t,

$$\langle \alpha_t \rangle = \frac{\int_0^{\alpha} d\alpha'\, \alpha' \,(\sum_{k=2}^{N-1} \hat{G}_{k,t}^2 Q_k^{2\,\alpha'})^{-N/2}}{\int_0^1 d\alpha'' \,(\sum_{k=2}^{N-1} \hat{G}_{k,t}^2 Q_k^{2\,\alpha''})^{-N/2}}, \tag{14}$$

its standard deviation $\delta\alpha = \sqrt{\langle \alpha_t^2 \rangle - \langle \alpha_t \rangle^2}$ with,

$$\langle \alpha_t^2 \rangle = \frac{\int_0^1 d\alpha' \,(\alpha')^2 \,(\sum_{k=2}^{N-1} \hat{G}_{k,t}^2 Q_k^{2\,\alpha'})^{-N/2}}{\int_0^1 d\alpha'' \,(\sum_{k=2}^{N-1} \hat{G}_{k,t}^2 Q_k^{2\,\alpha''})^{-N/2}}, \tag{15}$$

the expected value of ΔG_t,

$$\langle \Delta G_t \rangle = \frac{\int_0^1 d\alpha' \sqrt{1/2 \left(\sum_{k=2}^{N-1} \hat{G}_{k,t}^2 .* Q_k^{2\,\alpha}\right) \left(\sum_{l=2}^{N-1} Q_l .^{-2\,\alpha}\right)} \,(\sum_{k=2}^{N-1} \hat{G}_{k,t}^2 Q_k^{2\,\alpha'})^{-N/2} \Gamma\Big(N/2 - 1/2\Big)}{\int_0^1 d\alpha'' \,(\sum_{k=2}^{N-1} \hat{G}_{k,t}^2 Q_k^{2\,\alpha''})^{-N/2} \Gamma\Big(N/2\Big)} \tag{16}$$

and the standard deviation $\delta(\Delta G_t) = \sqrt{\langle \Delta G_t^2 \rangle - \langle \Delta G_t \rangle^2}$

$$\langle \Delta G_t^2 \rangle = \frac{\int_0^1 d\alpha' \left(1/(N-2)\sum_{k=2}^{N-1} \hat{G}_{k,t}^2 . * Q_k^{2\,\alpha}\right) \left(\sum_{l=2}^{N-1} Q_l .^{-2\,\alpha}\right) \left(\sum_{k=2}^{N-1} \hat{G}_{k,t}^2 Q_k^{2\,\alpha'}\right)^{-N/2}}{\int_0^1 d\alpha'' \left(\sum_{k=2}^{N-1} \hat{G}_{k,t}^2 Q_k^{2\,\alpha''}\right)^{-N/2}}. \tag{17}$$

IV. TEMPORAL CORRELATIONS

To quantify temporal correlations, we detrended growth from growth spatial patterns and we calculated Kendall's correlation coefficient.

A. Detrending

Before estimating time correlations, we corrected cellular growth using a local average of growth, aiming to detrend our estimate from large-scale deterministic spatial variations. We thus avoid potential bias induced by large scale growth variations that should not be considered as fluctuations. We use growth rate $G_{i,t}$ of cell i between t and $t+1$, as defined in Sec. II A. Computing local excess of growth is equivalent to apply a smooth Laplace operator to growth [1]. For convenience, we use the Laplace operator defined in (7), and we define $\delta G_{i,t} = \sum_j L_{ij,t} \sqrt{S_{j,t}/S_{i,t}} G_{j,t}$, where j spans cells that can be tracked from t to $t+2$. Detreneded growth at time t needs to be compared to detrended growth at time $t+1$, $\delta G_{J_{i,t},t+1} = \sum_{k \in J_{i,t}} \sum_j L_{kj,t+1} \sqrt{S_{k,t+1} S_{j,t+1}} G_{j,t+1} / (\sum_{l \in J_{i,t}} S_{l,t+1})$.

B. Kendall's correlation coefficient

Time correlations are quantified by Kendall's correlation coefficient Γ_t between $\delta G_{i,t}$ and $\delta G_{J_{i,t},t+1}$. We used a bootstrap approach with 10^4 resamplings to quantify the statistical properties of Γ_t. We estimated Γ_t from the median of the boostrap distribution and the bounds of the confidence interval are its 5^{th} and its 95^{th} percentile. Finally, we also considered $\langle \Gamma_t \rangle$ and $\delta\Gamma_t$ the expected value and the standard error of the distribution.

V. ANALYSIS OF TEMPORAL VARIATIONS IN GROWTH PAREMETERS

We analyzed two datasets, the first containing wild-type and mutant plants while the second group contained wild-type plants grown in different conditions. We first synchronised the time series of the two datasets. We then compared mutants to wild-type sepals from plants cultured in the same conditions, or wild type sepals from plant cultured in different conditions.

A. Registration

To synchronize (register) the different time series (labeled with an upper index (n)), we looked for the temporal shifts $\Delta t^{(n)}$ that maximise the overlap of curves of width vs. time $w_t^{(n)}$. The perfect overlap being, in general, not possible, we define a distance between pairs of curves, and we choose the delays which minimise the quadratic sum over all possible pairs $S = \sum_{n,n'} d_{nn'}^2$, of these distances. For two time series $w_t^{(n)}$ and $w_t^{(n')}$, the distance from n to n' is defined as $d_{nm} = A_{nn'} - A_{n'n}$, where $A_{nn'}$ is the area of the region in the Cartesian plane that is delimited to the left by the linear interpolation of $w_t^{(n)}$ versus t and to the right by the linear interpolation of $w_t^{(n')}$ versus t. This distance depends linearly on the the time-shifts, $d_{nn'} = a_{nn'} - a_{n'n} + h_{nn'}(\Delta t^{(n')} - \Delta t^{(n)})$ where $a_{nn'}$ and $a_{n'n}$ are the areas $A_{nn'}$ and $A_{n'n}$ before synchronization. The minimization problem is then simply quadratic and the shifts are the solution of

$$\sum_{n'} M_{nn'} \Delta t^{(n')} = Y_n,$$

with $M_{nn'} = \delta_{nn'}(\sum_m h_{nm}) - h_{nn'}$ and $Y_n = 2\sum_{n'}(a_{nn'} - a_{n'n}) h_{nn'}$. The matrix M is not invertible due to invariance by translations in time, but this system can be solved by adding the condition that the smallest temporal shift (the

smallest $\Delta t^{(n)}$) has a value of 0. We denote by $T_t^{(n)}$ the new temporal coordinate for live-imaging series n following registration.

B. Differences between mutant and wild-type growth parameters

To compare a quantity Φ_t (which could be Γ_t, ΔG_t, α_t or $\overline{G}_t = (\sum_i \sum_{j\in J_{i,t}} S_{j,t+1})/(\sum_i S_{i,t}) - 1)$ between mutant and wild-type sepals in dataset 1, we defined the mean difference D as,

$$D = \frac{\sum_{n',t'} \sum_{n,t} W_{t't}^{(n',n)} (\Phi_{t'}^{(n')} - \Phi_t^{(n)})}{\sum_{n',t'} \sum_{n,t} W_{t't}^{(n',n)}} \tag{18}$$

where the upper indices (n') and (n) label the mutant and wild-type live-imaging sequences, respectively. The sums $\sum_{n',t'}$ and $\sum_{n,t}$ are over all the time points of the mutant and the wild-type,respectively. D quantifies how much, on average, the quantities Φ_t for the mutants differ from the WT. The weights $W_{t',t}^{(n',n)}$ are defined as

$$W_{t',t}^{(n',n)} = \Lambda(T_{t'}^{(n')} - T_t^{(n)}), \tag{19}$$

where $\Lambda(x) = \max(1 - |x|, 0)$ is the triangle function. This definition ensures that only differences between mutants and WT of comparable stages are considered in the distance D.

Approximating the distribution of Φ_t to Gaussian, D has a Gaussian distribution and its expected value is

$$\langle D \rangle = \frac{\sum_{n,t} \sum_{n',t'} W_{t',t}^{(n',n)} (\langle \Phi_{t'}^{(n')} \rangle - \langle \Phi_t^{(n)} \rangle)}{\sum_{n,t} \sum_{n',t'} W_{t',t}^{(n',n)}},$$

where $\langle \Phi_{t'}^{(n')} \rangle$ and $\langle \Phi_t^{(n)} \rangle$ are the expected values of Φ for the mutants and the wild-type tissues. The standard deviation is

$$\delta D = \frac{\sqrt{\sum_{n,t} \sum_{n',t'} W_{t',t}^{(n',n)} \left(\left(\delta \Phi_{t'}^{(n')} \right)^2 - \left(\delta \Phi_t^{(n)} \right)^2 \right)}}{\sum_{n,t} \sum_{n',t'} W_{t',t}^{(n',n)}},$$

where $\delta \Phi_{t'}^{(n')}$ and $\delta \Phi_t^{(n)}$ are the standard error of Φ for the mutants and the WT tissues. We used the same method to compare between wild-type sepals from the two culture conditions.

VI. LINEAR FIT AND RESIDUALS

We used statistical inference to determine which linear relation is the most likely to fit our data. We did this to test if the master curve of Γ_t as function $\Delta t/\tau_t$ can well be fitted by a linear relation. In using statistical inference, we accounted for the strong uncertainty of the different estimates we made. We could also estimate the uncertainty of the fit itself end test whether the distribution of data around the fit can be explained by the data uncertainty, in coherence with the hypothesis of a linear and deterministic relation between the two. This is what we did in a second time.

A. Linear fit

We did this analysis to fit the master curve Γ_t as function of $\Delta t/\tau_t$ but since we applied the same analysis to other scatter plots, we preferred to consider genera $x-$ and $y-$coordinates. In a method which account for the uncertainty of the data estimates. To each measurement performed (indexed i) is associated a probability $p_i(x_i, y_i)$ of finding a certain quantity x_i associated to the quantity y_i. Approximating p_i to a Gaussian distribution, and assuming not specific correlations for the error on x_i and y_i, we can write

$$p_i(x_i,y_i)=\exp\left(-1/2\left(\frac{(x_i-\langle x_i\rangle)^2}{\delta x_i^2}+\frac{(y_i-\langle y_i\rangle)^2}{\delta y_i^2}\right)\right)/(2\pi\delta x_i\delta y_i), \tag{20}$$

where $\langle x_i\rangle$ and $\langle y_i\rangle$ are the expected values of x_i and y_i and δx_i, and δy_i are their standard errors. The probability of finding the x-coordinate in x_i and of being on the line $y=\beta_0+\beta_1 x$ is then, $p_i(x_i,\beta_0+\beta_1 x_i)$ which can be written as

$$p_i(x_i,\beta_0+\beta_1 x_i)=\exp\left(-1/2\left(\left(\frac{1}{\delta x_i^2}+\frac{1}{\delta y_i^2}\right)\left(x-\beta_1\frac{\langle y_i\rangle-\beta_0-\beta_1\langle x_i\rangle}{\delta y_i^2+\beta_1^2\delta x_i^2}\right)^2+\frac{(\langle y_i\rangle-\beta_0-\beta_1\langle x_i\rangle)^2}{\delta y_i^2+\beta_1^2\delta x_i^2}\right)\right)/(2\pi\delta x_i\delta y_i), \tag{21}$$

where we rearranged the argument of the exponential to write the dependence with x as a square. Integrating over x_i, we obtain the probability that the data measured in i falls on the line $y=\beta_0+\beta_1 x$ as

$$p_i(y=\beta_0+\beta_1 x)=e^{-1/2\frac{(\langle y_i\rangle-\beta_0-\beta_1\langle x_i\rangle)^2}{\delta y_i^2+\beta_1^2\delta x_i^2}}/\sqrt{2\pi(\delta y_i^2+\beta_1^2\delta x_i^2)}, \tag{22}$$

The probability of having the n, assumed independent, measurements falling on $y=\beta_0+\beta_1 x$ is then $\prod_{i=1}^n p_i(y=\beta_0+\beta_1 x)$, and using flat prior for β_0 and a Cauchy distribution as a prior for β_1, which is equivalent to assume a flat prior for the orientation of the line $y=\beta_0+\beta_1 x$, we get

$$P(\beta_0,\beta_1)=\frac{e^{-1/2\sum_{i=1}^n\frac{(\langle y_i\rangle-\beta_0-\beta_1\langle x_i\rangle)^2}{\delta y_i^2+\beta_1^2\delta x_i^2}}}{Z(1+\beta_1^2)\sqrt{2\pi}\prod_{i=1}^n\sqrt{\delta y_i^2+\beta_1^2\delta x_i^2}} \tag{23}$$

where the constant Z given below is defined so that $\int_{-\infty}^{+\infty}d\beta_0\int_{-\infty}^{+\infty}d\beta_1 P(\beta_0,\beta_1)=1$. Introducing $a(\beta_1)=\sum_{i=1}^n 1/(\delta y_i^2+\beta_1^2\delta x_i^2)$, $b(\beta_1)=\sum_{i=1}^n(\beta_1\langle x_i\rangle-\langle y_i\rangle)/(\delta y_i^2+\beta_1^2\delta x_i^2)$, $c(\beta_1)=\sum_{i=1}^n(\beta_1\langle x_i\rangle-\langle y_i\rangle)^2/(\delta y_i^2+\beta_1^2\delta x_i^2)+\log(\delta y_i^2+\beta_1^2\delta x_i^2)$, we can write

$$P(\beta_0,\beta_1)=\frac{e^{-1/2(\beta_0^2 a(\beta_1)+2\beta_0 b(\beta_1)+c(\beta_1))}}{Z(1+\beta_1^2)}. \tag{24}$$

Then, $Z=\int_{-\infty}^{+\infty}d\beta_0\int_{-\infty}^{+\infty}d\beta_1\frac{e^{-1/2(\beta_0^2 a(\beta_1)+2\beta_0 b(\beta_1)+c(\beta_1))}}{(1+\beta_1^2)}$ can be rewritten, computing the first integral, as

$$Z=\int_{-\infty}^{+\infty}d\beta_1\frac{e^{-1/2(c(\beta_1)-b(\beta_1)^2/a(\beta_1))}}{(1+\beta_1^2)\sqrt{a(\beta_1)}}. \tag{25}$$

The expected value for β_1 is thus

$$\langle\beta_1\rangle=\int_{-\infty}^{+\infty}d\beta_1\beta_1\frac{e^{-1/2(c(\beta_1)-b(\beta_1)^2/a(\beta_1))}}{Z(1+\beta_1^2)\sqrt{a(\beta_1)}}. \tag{26}$$

and the standard deviation is $\delta\beta_1=\sqrt{\langle\beta_1^2\rangle-\langle\beta_1\rangle^2}$, where

$$\langle\beta_1^2\rangle=\int_{-\infty}^{+\infty}d\beta_1\beta_1^2\frac{e^{-1/2(c(\beta_1)-b(\beta_1)^2/a(\beta_1))}}{Z(1+\beta_1^2)\sqrt{a(\beta_1)}}. \tag{27}$$

The expected value for β_0 is

$$\langle\beta_0\rangle=-\int_{-\infty}^{+\infty}d\beta_1\frac{b(\beta_1)}{a(\beta_1)}\frac{e^{-1/2(c(\beta_1)-b(\beta_1)^2/a(\beta_1))}}{Z(1+\beta_1^2)\sqrt{a(\beta_1)}}, \tag{28}$$

and the standard deviation $\delta\beta_1=\sqrt{\langle\beta_1^2\rangle-\langle\beta_1\rangle^2}$, where

$$\langle\beta_0^2\rangle=\int_{-\infty}^{+\infty}d\beta_1\left(\frac{1}{a(\beta_1)}+\left(\frac{b(\beta_1)}{a(\beta_1)}\right)^2\right)\frac{e^{-1/2(c(\beta_1)-b(\beta_1)^2/a(\beta_1))}}{Z(1+\beta_1^2)\sqrt{a(\beta_1)}}. \tag{29}$$

We computed these integrals numerically to estimate the fitting parameters and their standard deviations.

B. residuals

We would like to test if the expected values $\langle\beta_0\rangle$ and $\langle\beta_1\rangle$ allow to adequately fit the set of data. We gave in (22) the probability of having a linear relation $y = \beta_0 + \beta_1 x$ in the measurement i. For $\beta_0 = \langle\beta_0\rangle$ and $\beta_1 = \langle\beta_1\rangle$, it is,

$$p_i(y = \langle\beta_0\rangle + \langle\beta_1\rangle x) = e^{-1/2\frac{(\langle y_i\rangle - \langle\beta_0\rangle - \langle\beta_1\rangle\langle x_i\rangle)^2}{\delta y_i^2 + \langle\beta_1\rangle^2\delta x_i^2}} / \sqrt{2\pi(\delta y_i^2 + \langle\beta_1\rangle^2\delta x_i^2)}, \tag{30}$$

We see that this probability follows a standard normal distribution with respect to the parameter $r_i = \frac{(\langle y_i\rangle - \langle\beta_0\rangle - \langle\beta_1\rangle\langle x_i\rangle)^2}{\delta y_i^2 + \langle\beta_1\rangle^2\delta x_i^2}$. If our assumptions are consistent, and notably the assumption that a linear relation exists between y_i and x_i is correct, then the distribution of r_i over all the measurements should be close to a standard normal distribution. To assess this, we performed a Kolmogorow-Smirnov test. We concluded that, in the case of the master curve, the distribution of data around the fit can be explained by the uncertainty on the estimates, and that the data are compatible with the hypothesis of a linear and deterministic relation between Γ_t and $\Delta t/\tau_t$, while we could not draw the same conclusions for any of the other pairwise trends.

[1] Antoine Fruleux and Arezki Boudaoud. Cellular fourier analysis for geometrically disordered materials. *Physical Review Research*, 3(2):023036, 2021.

[2] D Engwirda. Unstructured mesh methods for the navier-stokes equations. *Undergraduate Thesis, School of Engineering, University of Sidney*, 2005.

[3] Darren Engwirda. Locally optimal delaunay-refinement and optimisation-based mesh generation. 2014.